

1 **Development of a dynamic dust-source map for NMME-DREAM v1.0 model based on MODIS**
2 **NDVI over the Arabian Peninsula**

3 Solomos Stavros^{1,2}, Abdelgadir Abuelgasim^{2*}, Christos Spyrou³, Ioannis Biniotoglou⁴, Slobodan
4 Nickovic⁵

5 **Abstract** We developed a time dependent dust source map for NMME-DREAM v1.0 model
6 based on the satellite MODIS Normalized Difference Vegetation Index (NDVI). Areas with
7 NDVI<0.1 are classified as active dust sources. The updated modeling system is tested for dust
8 emission capabilities over SW Asia using a mesoscale model grid increment of 0.1°×0.1° km for
9 a period of one year (2016). Our results indicate significant deviations in simulated Aerosol
10 Optical Depths compared to the static dust-source approach and general increase in dustloads
11 over the selected domain. Comparison with MODIS Aerosol Optical Depth (AOD) indicates a
12 more realistic spatial distribution of dust in the dynamic source simulations compared to the
13 static dust sources approach. The modeled AOD bias is improved from -0.140 to 0.083 for the
14 case of dust events (i.e. for AOD >0.25) and from -0.933 to -0.424 for dust episodes with
15 AOD>1. This new development can be easily applied to other time periods, models and
16 different areas worldwide for a local fine tuning of the parameterization and assessment of its
17 performance.

18 ¹ Institute for Astronomy, Astrophysics, Space Applications and Remote Sensing (IAASARS), National Observatory of Athens,
19 Athens, Greece, stavros@noa.gr

20 ² Department of Geography and Urban Planning, National Space Science and Technology Center, United Arab Emirates
21 University

22 ³ Department of Geography, Harokopio University of Athens (HUA), El. Venizelou Str. 70, 17671 Athens, Greece.

23 ⁴ National Institute of R & D for Optoelectronics, Magurele, Ilfov, Romania

24 ⁵ Republic Hydrometeorological Service of Serbia , Belgrade, Serbia

25 *Corresponding author

26 **Keywords:** dust, Arabian Peninsula, DREAM, NDVI, model, satellite

27 **Introduction**

28 The importance of natural particles, namely desert dust, in the weather and climate has
29 been underlined in a great number of studies. Dust is a climatic regulator, as it modifies
30 extensively the radiative balance of the atmospheric column (e.g. Torge et al., 2011; Spyrou et
31 al., 2013; Mahowald et al., 2014). At the same time dust aerosols modify the atmospheric water
32 content (Spyrou 2018), the way clouds are formed by acting as cloud condensation nuclei (CCN)
33 and ice nuclei (IN) and the precipitation process (Kumar et al., 2011; Solomos et al., 2011;
34 Nickovic et al., 2016). In addition, there is a clear connection between dust particles and human
35 health disorders, as the size of the produced aerosols is small enough to cause respiratory and
36 cardiovascular diseases, as well as pathogenic conditions due to the microorganisms that they
37 can potentially carry (Mitsakou et al., 2008; Esmail et al., 2014).

38 The Arabian Peninsula is one of the most important sources of mineral dust worldwide and
39 contributes together with the Saharan and Gobi Deserts in the formation of a North
40 Hemisphere “dust belt” as described by Prospero et al. (2002). Severe dust storms over the
41 Peninsula are quite common, especially during long periods without rain, in the spring and
42 summer (Almazrouia et al., 2012). Particles injected into the atmosphere from arid soils, under
43 favorable weather conditions (high wind speeds and dry soil), can affect large areas around the
44 sources but also remote locations like the Eastern Mediterranean (Mamouri et al., 2016;
45 Solomos et al., 2017) and the Indian Ocean (Chakraborty et al. 2006).

46 Due to the multitude and severe effects of dust particles not only on the weather and the
47 ecosystem but to human health as well, the proper description of the production, transport and
48 eventual deposition of the dust cycle, in numerical weather prediction models (NWP) is
49 essential. In order to be able to accurately describe the dust life-cycle in the atmosphere, we
50 need a clear understanding of the areas which can potentially act as “dust sources”. The
51 definition of such areas dictates the emission strength and therefore the amount of particles
52 inserted into the atmosphere. A proper representation of dust sources is therefore an essential
53 first step, in studying the impacts of mineral particles in the climate and human societies.
54 Usually the definition of the areas that can act as dust sources is made using global datasets.
55 For example Nickovic et al. (2001) used a subjective correspondence between the Olson World
56 Ecosystems (Olson et al., 1983) and the thirteen SSib (simplified simple biosphere, Xue et al.
57 1991) vegetation types to identify arid and semi-arid areas. Similarly, Spyrou et al., (2010) used
58 a 30sec global land use/cover database, classified according to the 24 category U.S. Geological
59 Survey (USGS) land use/cover system (Anderson et al., 1976), to define active areas in SKIRON
60 dust model. Solomos et al., (2011) used the LEAF soil and vegetation sub-model of the Regional
61 Atmospheric Modeling System (RAMS) (Walko et al., 2000) to identify the active dust sources in
62 RAMS-ICLAMS model.

63 However, the above mentioned methodologies have some significant drawbacks. The
64 datasets are usually not up-to-date, therefore recent land-use modifications are not included
65 and not represented. In addition, such “static” databases mean that possible seasonal
66 variations are not taken into account. Towards the direction of overcoming the above
67 limitations and improving global dust forecasts, Kim et al., (2013) developed a dynamical dust
68 source map for the GOCART dust model by characterizing NDVI values < 0.15 as active dust
69 spots. Similarly Vukovic et al., (2014) combined MODIS landcover types with pixels having NDVI
70 < 0.1 to identify the seasonal dust sources that enforced the severe Phoenix haboob of July
71 2011 in the US. Such information can be even more relevant at meso and local scales for
72 determining landuse changes and potential dust sources, especially in heterogeneous regions
73 such as the Arabian Peninsula (which has more diverse soil types than e.g. the Sahara Desert)
74 and the greater SW Asia. In this context, Solomos et al., (2017), used the Landsat-8 NDVI data
75 (assuming also NDVI < 0.1 as active sources) to identify recent changes in landuse due to the war
76 in Iraq and Syria resulting in a significantly more realistic simulation of dust properties in the
77 Middle East.

78 In the current study we present the implementation of a dynamical dust source map in the
79 well-established and widely used DREAM v1.0 dust model (Nickovic et al., 2001; Perez et al.,
80 2006). The new development is first tested here for the greater SW Asia but can be extended
81 for use in mesoscale dust modeling applications worldwide. Two experimental simulations are

82 performed for one month period (August 2016) over the greater SW Asia: 1) Control run, where
 83 the dust source definition is based on the Ginoux et al., (2001) dataset and 2) Dynamic source
 84 run, where the NDVI values are used to identify the dust sources. The main differences in our
 85 approach compared to the previous studies referenced above, is that we use a very high
 86 resolution NDVI product (500x500 m) in a regional modeling domain (e.g. Kim et al., 2013 used
 87 an 8x8 Km NDVI dataset extrapolated to 1°x1° global modeling domain) and our study is not
 88 limited to specific test cases (like for example Vukovic et al., 2014 and Solomos et al., 2017),
 89 but covers an extended time period, as presented below. The model results from both runs are
 90 compared to available satellite observations and station measurements inside the modeling
 91 domain. In section 1 we describe the methodological steps regarding the model developments
 92 and remote sensing data; Section 2 includes the results of the experimental runs and section 3
 93 is a summary and discussion of the study findings.

94
 95

96 **1. Methodology**

97

98 **1.1. Model description**

99 The modeling system used in this study is NMME-DREAM v1.0. The meteorological core is
 100 the NCEP/NMME atmospheric model (Janjic et al., 2001). The Dust Regional Atmospheric Model
 101 (DREAM v1.0) is a numerical model created with the main purpose to simulate and predict the
 102 atmospheric life-cycle of mineral dust using an Euler-type nonlinear partial differential equation
 103 for dust mass continuity (Nickovic et al., 2001; Perez et al., 2006; Pejanovic et al., 2011, Nickovic
 104 et al., 2016). In DREAM the concentration approach is used for dust uplift, where surface
 105 concentration is used as a lower boundary condition and used for the calculation of surface
 106 fluxes, which in turn depends of the friction velocity (Nickovic et al., 2001). This surface
 107 concentration is calculated using equation (11) from Nickovic et al., (2001):

108

$$109 \quad C_{sfc} = c_1 \cdot \delta \cdot u_*^2 \left[1 - \left(\frac{u_{*t}}{u_*} \right)^2 \right] \quad \text{where } c_1 = 2.4 \cdot 10^{-4} \frac{Kgr}{m^5 \text{ sec}^2} \text{ a constant determined from model}$$

110 experiments, u_* and u_{*t} the friction velocity and the threshold friction velocity for dust
 111 production respectively and $\delta = a \cdot \gamma_k \cdot \beta_k$, where γ_k the ratio between the mass available for
 112 uplift and the total mass β_k the fractions of clay, silt and sand for each soil class, and a the
 113 desert mask (between 0 and 1) calculated from the Ginoux et al., (2001) dataset. Soil moisture
 114 and particle size dictate the threshold friction velocity which initializes dust production. Once
 115 particles have been lifted from the ground they are driven by the atmospheric model variables
 116 and processes. Therefore turbulent parameters are used in the beginning of the process, when
 117 dust is lifted from the ground, and transported by model winds in the later phases when dust
 118 travels away from the sources. The model handles dust in eight size bins, with effective radii of
 119 0.15, 0.25, 0.45, 0.78, 1.3, 2.2, 3.8, and 7.1 μm . Dust is treated as a passive tracer and doesn't
 120 interact with radiation or clouds. Dust is eventually settled through rainfall and/or dry
 121 deposition processes parameterized according to the scheme of Georgi (1986) which includes

122 deposition by surface turbulent and Brownian diffusion, gravitational settling and impact on
123 surface elements.

124 In order to test the use of NDVI for source characterization, the model is setup with a horizontal
125 resolution of 0.1°x0.1°, covering the Arabian Peninsula parts of SW Asia and parts of NE Africa
126 (Figure 1). On the vertical we use 28 levels stretching from the surface to the top of the
127 atmosphere. August 2016 has been selected as a test period for the model development due to
128 the significant dust activity and variability in wind properties during this month. One-year runs
129 for the entire 2016 have been conducted to evaluate the performance of the static and
130 dynamic database emission maps. The original classification of dust sources in DREAM is based
131 on Ginoux et al., (2001) that takes into account the preferential sources related to topographic
132 depressions and paleolake sediments. The global mapping of dust sources in Ginoux et
133 al.,(2001) is determined from the comparison between the elevation of surface grid points at
134 1°x1° resolution with the surrounding hydrological basins and with the 1°x1° AVHRR (Advanced
135 Very High Resolution Radiometer) vegetation map (DeFries and Townshend, 1994). Recent
136 studies indicated the contribution of both natural and anthropogenic dust sources to the overall
137 dust emissions detected in MODIS Deep Blue product (Ginoux et al., 2012) and also the
138 relevance of local geomorphological conditions and sediment supply (Parajuli and Zender,
139 2017) on the global dust emissions. All these advances in dust emissions are based on static
140 map considerations.

141 In our work, a numerical procedure has been developed to insert the NDVI satellite information
142 into the model and to update such info each time the NDVI changes, during the simulation
143 period. We assume that regions with NDVI values from 0 to 0.1 correspond to bare soil and
144 therefore can be efficient sources (“dust points”; DeFries and Townshend, 1994; Solomos et al.,
145 2017). In general it is not easy to define a global threshold value for all satellite NDVI sensors
146 and all vegetation types worldwide. For example Kim et al. (2013) used a threshold of 0.15 to
147 define global dust sources based on AVHRR retrievals (Tucker et al., 2005; Brown et al., 2006).
148 Here we adopt the 0.1 NDVI threshold due to the bareness of the specific modeling domain
149 since a higher value could overestimate the regional dust sources. The NDVI dataset is at finer
150 resolution than the model grid (500x500 m) and in order to find the potential for dust
151 production in each model grid box, we calculate the following ratio:

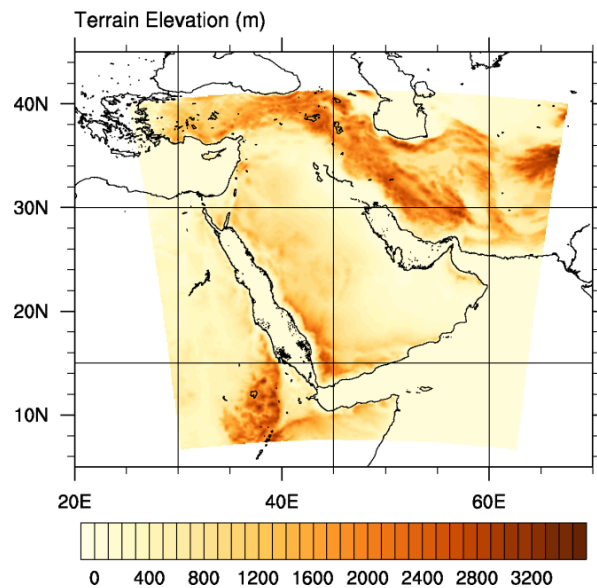
$$A_{grid_box} = \frac{\#_of_dust_point\ s}{Total_#_of_point\ s}$$

152 Where $\#_of_dust_point\ s$ is the number of points with NDVI values smaller than 0.1. This
153 approach allows for a dynamic description of dust source areas over the model domain to
154 replace the previously used static database. Moreover, the scaling of satellite data over model
155 grid points allows the use of the same algorithm for different model configurations. Several
156 mountains in the area (e.g. the Sarawat Mountains along the Red Sea coast and the Zagros
157 Mountains in Iraq) could be misclassified as dust sources due to low NDVI values. In order to
158 exclude such unrealistic emissions from non-soil bare areas or snow-covered areas we have
159 applied a limit of zero dust production above 2500 m over the entire domain. This simple
160 approach has been selected in order to keep our straightforward NDVI mapping independent of
161 vegetation and soil information. The threshold value of 2500 m does not suppress the
162

163 emissions from lowlands and hillsides (e.g. the coastal areas of Hejaz Mountains in Red Sea that
164 have been identified as hot dust spots by Anisimov et al., 2017).

165 In Figure 2a we show the static sources in the original model version with a factor of 0 to 1
166 depending on the source area strength. Accordingly in Figure 2b we show the new dynamic
167 sources for 1-16 of August 2016. The two dust source patterns present remarkable difference
168 especially over the western Saudi Arabia and over Iran and Pakistan where the NDVI
169 classification results in stronger emissions. In order to test the performance of the new
170 methodology we run the model in two different configurations: (1) Using the static Ginoux et
171 al., (2001) dust source database, called DREAM-CTRL run from now on, and (2) using the
172 dynamic NDVI database as described above, called DREAM-NDVI run from now on. Both setups
173 are initialized using the NCEP GFS analysis files (0.5°×0.5° at 00, 06, 12 and 18 UTC), which were
174 used for boundary conditions as well. The two model configurations are identical other than the
175 dust source database.

176



177

178

Figure 1: DREAM model domain and topography in meters

179

1.2 NDVI description

180

181

182

183

184

185

186

187

188

189

For the purposes of our study we used the 500m 16-day averaged NDVI from MODIS (Didan, 2015) for the period of interest. The NDVI is a normalized transform of the near infrared to red reflectance ratio, designed to provide a standard for vegetation and takes values between -1 and +1. Since it is expressed as a ratio, the NDVI has the advantage of minimizing certain types of band-correlated noise (positively-correlated) and influences attributed to variations in irradiance, clouds, atmospheric attenuation and other parameters (Solano et al., 2010).

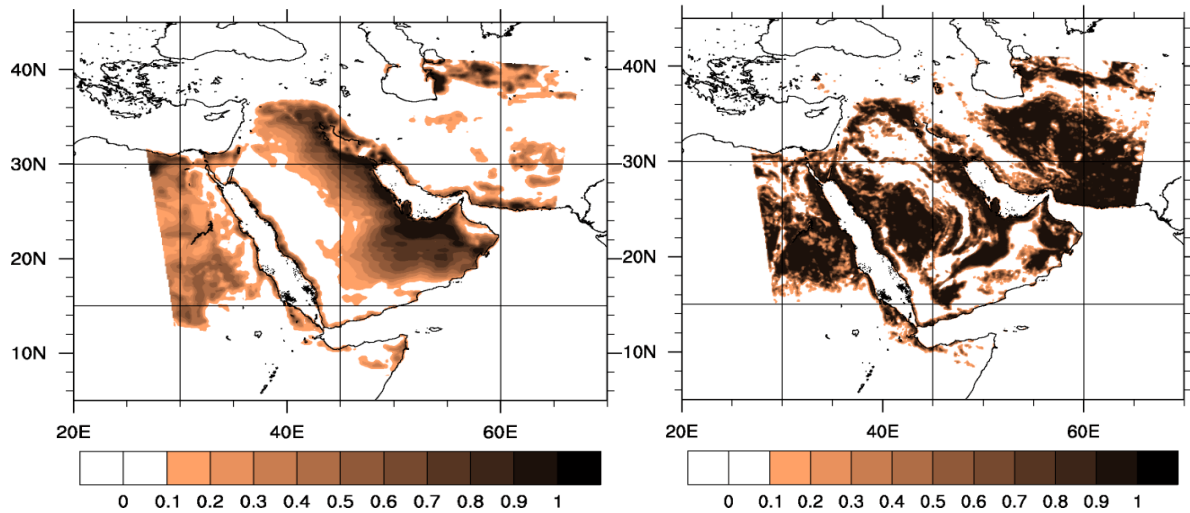
To create an accurate time-dependent dust source map, we have utilized the Normalized Difference Vegetation Index (NDVI) derived from the MODIS/Terra instrument. NDVI is calculated as the normalized difference of reflectance in the red and near-infrared channels (Rouse et al., 1974; Huete et al. 2002) i.e.,

190

$$NDVI = \frac{X_{nir} - X_{red}}{X_{nir} + X_{red}}$$

191 where X represents surface reflectance as would be measured at ground level (i.e. corrected for
 192 atmospheric gas and aerosol effects).in each channel. The 16-day composite is calculated by
 193 ingesting two 8-day composite surface reflectance granules, taking into account pixel quality,
 194 presence of clouds, and viewing geometry. This procedure can lead to spatial discontinuities, as
 195 it is possible that data from different days are used for adjacent pixels, each representing
 196 different measurement conditions. If a pixel had no useful measurements during the 16-day
 197 period, historic data are used as fill values (Didan et al., 2015). For terrestrial targets, NDVI will
 198 take values near 0.8 for vegetated areas and near 0 for barren soil (Huete et al., 1999). The
 199 high-resolution dataset was used to calculate the percentage of barren land in each 0.1°x0.1°
 200 model grid cells and this percentage was used to define the effective strength of dust sources in
 201 each cell.

202



203
 204
 205
 206
 207

Figure 2: Dust source strength as defined by (a) the Ginoux et al., 2001 dataset and (b) the 16th of August 2016 mean NDVI

208 **1.3 Evaluation datasets and metrics**

209 Model evaluation is carried out two datasets. First, the MODIS monthly aerosol optical depth
 210 (AOD) is use to study the spatial distribution of dust in the model domain. For this we use the
 211 level 3 gridded atmosphere monthly product at 1x1 resolution, MOD08_ME (Platnick et al.
 212 2017). Secondly, we evaluate model performance using AERONET AOD retrievals at 8
 213 photometric stations. AERONET is a network of sun/sky photometers that derive aerosol
 214 optical and microphysical properties at a large number of stations around the world (Holben et
 215 al., 1998). For this evaluation, we use Version 3 AOD retrievals that, in comparison with
 216 previous versions, improves automatic cloud screening (Giles et al, 2018). Level 2 datasets were
 217 used for all stations apart from Kuwait University, where only Level 1.5 data were available.
 218 Both model and AERONET AOD were calculated at 532nm; this was chosen to facilitate future
 219 intercomparing against lidar systems that frequently measure at this wavelength (e.g.

220 Pappalardo et al., 2014). AERONET measurements were converted to this wavelength using the
221 440-870 angstrom exponent and taking into account AOD measurements at 440nm, 675nm,
222 and 870nm; in the cases where the 440nm AOD was not available, the 500nm (Mezaira) or
223 443nm (KAUST campus) measurement was used instead.

224

225 We evaluate model performance using five metrics: mean bias, root mean square error,
226 correlation coefficient, mean fractional bias, and fractional gross error. Concretely, assuming
227 we have n pairs of model values (m_i) and observations (o_i), the mean bias (MB) is defined as:

$$228 \quad MB = \overline{m_i - o_i}$$

229 where the bar denotes the mean value. Root mean square error (RMSE) is defined as

$$230 \quad RMSE = \sqrt{\overline{(m_i - o_i)^2}}$$

231 The correlation coefficient (r) is defined as

$$232 \quad r = \frac{\sum_{i=1}^n (m_i - \bar{m})(o_i - \bar{o})}{\sqrt{\sum_{i=1}^n (m_i - \bar{m})^2} \sqrt{\sum_{i=1}^n (o_i - \bar{o})^2}}$$

233 The fractional gross error (FGE) is defined as

$$234 \quad FGE = 2 \left| \frac{\overline{m_i - o_i}}{\overline{m_i + o_i}} \right|$$

235 following Boylan and Russell, 2006. Similarly, mean fractional bias (MFB) is defined as

$$236 \quad MFB = 2 \frac{\overline{m_i - o_i}}{\overline{m_i + o_i}}$$

237

238

239 following Chang and Hanna, 2004.

240

241

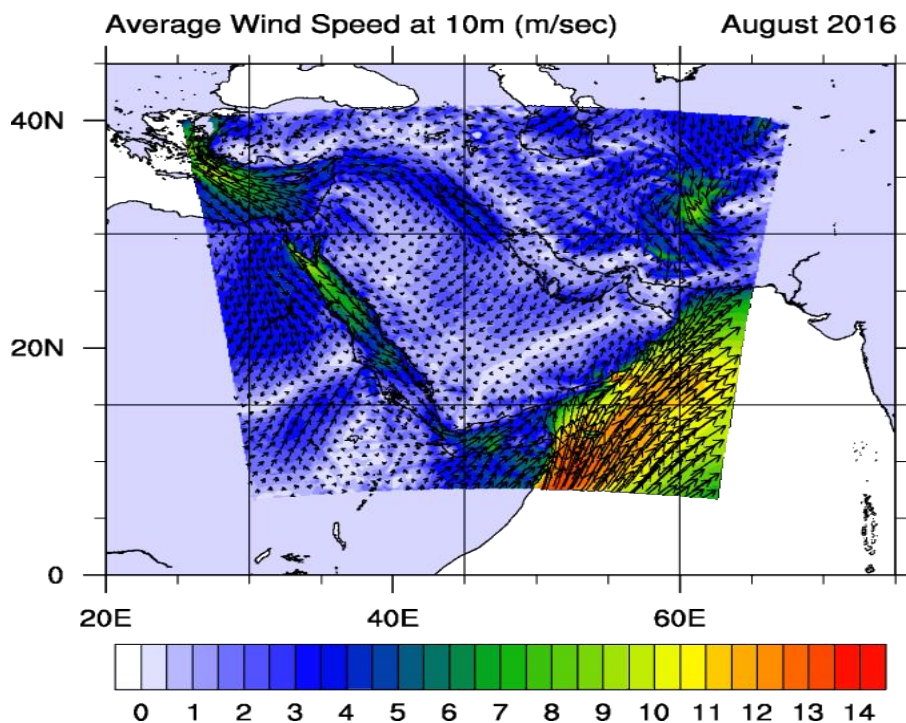
242 **2. Results**

243 DREAM-CTRL runDREAM-NDVI runThe test simulation period is 1-31 August 2016 and the
244 results from both simulations are compared to MODIS and AERONET AOD. A five days spin up
245 model run, prior to the experimental period, is used for establishing the dust background over
246 the domain. After finalizing the experimental model configuration we perform a complete one-
247 year run (2016) and evaluate the results against AERONET stations.

248 **2.1 Dust transport during August 2016**

249 The selected 1-month period is characterized by a significant variability in wind speeds and
250 directions (Figure 3) which allows the evaluation of the new model version under different
251 conditions. During 1-10 August, east winds prevail over the region and increased dust
252 concentrations are found mostly along the central, east and south coastal areas of the Arabian
253 Peninsula. An anticyclonic circulation is established during 10-15 over the Arabia Desert and
254 increased dust concentrations are mostly found over the central desert areas. On 16-26 August
255 the circulation is mainly from north directions and thick dust plumes are advected southwards

256 towards the Arabian Sea. The north winds veer to east on 26-31 August and increased
257 dustloads are found over the Gulf during these dates.



258
259 Figure 3. Average wind speed (color scale) and vectors from NMME-DREAMv1.0 for August
260 2016.

261 2.2 Comparison with MODIS and AERONET

262 The monthly average AOD for August 2016 is shown in Figure 4 for the two experimental runs
263 (Figure 4a,b). The DREAM-NDVI run results in a significantly modified spatial distribution of dust
264 presenting increased dustloads over the entire domain and most profoundly over the Red Sea
265 and Gulf regions (Figure 4b). This dust pattern is closer to the MODIS observed AOD over the
266 same period that is shown in Figure 4c. The MODIS AOD in this area is mostly related to dust,
267 however it must be taken into account that other aerosols not parameterized in the model (e.g.
268 sea salt, sulphates, nitrates) may also contribute to the observed MODIS AOD.

269 The first step is to examine how our methodology compares against the monthly average AOD
270 in our study area. Therefore the monthly average AOD values produced from our two
271 simulations (DREAM-NDVI run and DREAM-CTRL run) are compared. More specifically the
272 DREAM-NDVI run reproduces the MODIS observed AOD pattern that is in general characterized
273 by values 0.3-0.4 at the NW parts of the Arabian Peninsula and by values 0.4-0.8 at the SE parts.
274 Significant improvement is also evident over the Red Sea and NE Africa. The DREAM-NDVI run
275 captures the maximum observed AOD values reaching up to 1.6 over the Red Sea and also the
276 southwesterly extension of an AOD tongue of 0.3-0.8 towards Soudan. At the east parts of the
277 modeling domain the DREAM-NDVI run again outperforms the DREAM-CTRL run since it
278 reproduces the spatial distribution of AOD 0.4-0.8 over the Arabian Sea and the maximum of

279 0.8-1.2 at the SE edge of Arabian Peninsula. Inside the Gulf, the NDVI run correctly represents
280 the 0.4-0.8 AOD but the dust concentration is over-predicted at the Strait of Hormuz and along
281 the Iran - Pakistan coastline. This is mostly due to the prevailing NE winds during the last days of
282 the August 2016 modeling period and due to a possible miss-classification of Iran and Pakistan
283 grid points as effective dust sources thus favoring unrealistic southeasterly transport towards
284 the Gulf of Oman. The DREAM-NDVI AOD is also higher than MODIS AOD over western Saudi
285 Arabia indicating a possible overprediction of dust sources at this area.

286 As a second step we run the same model configurations (CTRL and NDVI) for the entire 2016.
287 The modeled dust optical depth is compared with individual AERONET measurements. The
288 model retrievals are interpolated in time to match the AERONET measurement time
289 considering only dust relevant measurements with Angström Coefficient <0.6 (Holben et al.,
290 1998) and the results are shown in Table 1. For completeness we first consider all AERONET
291 stations inside the modeling domain for the evaluation. However the stations that are at the
292 margins of our domain (Cairo_EMA_2, SEDE_BOKER, AgiaMarina_Xyliatou and El_Farafra) are
293 also affected by other dust source areas (e.g. Sahara Desert) and their statistics are not
294 representative for Arabian and Middle East sources. Instead, the comparison with Arabian
295 Peninsula stations (Eilat, Kuwait_University, KAUST_Campus and Mezaira) provides more
296 insight on the effects of the new source characterization. As seen in Figure 5 and also in Table 2
297 these stations are clearly benefited from the experimental run.

298 In general the two runs present a significant statistical difference and more remarkably a
299 reverse of bias (MODEL-AERONET) from negative in the DREAM-CTRL run to positive in the
300 DREAM-NDVI run. The DREAM-NDVI run produces increased AODs that are neither linearly
301 proportional to the DREAM-CTRL run AODs nor uniformly distributed over the domain. When
302 considering only Arabian stations, the statistical metrics in Table 1 and especially the fractional
303 gross error and bias are improved but the RMSE is increased due to the increase in maximum
304 modeled AODs. In order to investigate the sensitivity of our results towards the severity of dust
305 events we further assume two additional air quality states in Table 1: (i) dust events (AOD>0.25)
306 and (ii) severe dust episodes (AOD>1). Both cases show an improvement in the bias values over
307 the control simulations. When we consider AOD>1 the DREAM-NDVI run still underestimates
308 the observed values, but with a lower RMSE (0.586 versus 0.983 of the DREAM-CTRL run). This is
309 clearly evident in Figure 6 where the NDVI run is indeed more realistic for the Arabian stations
310 but still does not reproduce the extreme AOD during severe episodes. For most of the cases
311 such high AODs should be attributed to duststorms from convective downdrafts (haboobs).
312 These processes are not resolved at mesoscale model resolutions (Solomos et al., 2012, 2017;
313 Vukovic et al., 2014) and thus cannot be represented here.

314

315 **Table 1. Statistical metrics from the comparison between the annual runs and AERONET**

	Mean bias (Model-Observation)		RMSE		Correlation		Fractional gross error		Mean fractional bias	
	CTRL	NDVI	CTRL	NDVI	CTRL	NDVI	CTRL	NDVI	CTRL	NDVI
AOD > 0 (All Stations)	-0.163	0.015	0.258	0.312	0.408	0.464	0.887	0.803	-0.639	0.043
AOD > 0 (Arabia Stations)	-0.142	0.122	0.252	0.332	0.340	0.426	0.644	0.515	-0.455	-0.187
AOD > 0.25 (Arabia Stations)	-0.140	0.083	0.283	0.350	0.238	0.328	0.640	0.462	-0.527	-0.142
AOD > 1 (Arabia Stations)	-0.933	-0.424	0.983	0.586	0.032	0.009	1.230	0.481	-1.211	-0.413

The AERONET stations used in this study are: Eilat (29N,34E), Cairo_EMA_2 (30N,31E), Kuwait_University (29N,47E), KAUST_Campus (22N,39E), SEDE_BOKER (30N,34E), AgiaMarina_Xyliatou (35N,33E), Mezaira (23N,53E) and El_Farafra (27N,27E)

316 **3. Summary and Discussion**

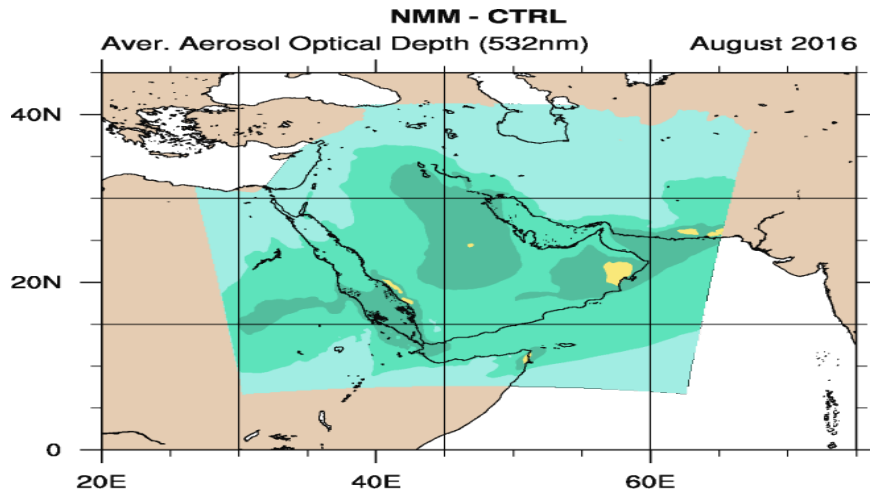
317 In this study we present the development of a dynamic dust source map for implementation in
 318 NMME-DREAM v1.0 over the Arabian Peninsula and the greater areas of Middle East, SW Asia
 319 and NE Africa. Although the major dust sources worldwide are located in permanent deserts
 320 where the NDVI is almost always <0.1 (e.g. Bodele Depression, Gobi Desert, Arabian Desert),
 321 the dynamical scaling of dust emissions presented here can be important for providing up-to-
 322 date evidence of active dust sources over non-permanent deserts. These may include dried
 323 bog, marshes and semi-desert areas as well as irrigated and non-irrigated farms where landuse
 324 changes occur throughout the year. Analysis of the modeling results for one year test period
 325 (2016) over SW Asia indicated the improved performance of the new parameterization. The
 326 DREAM-NDVI run showed a significant increase in dustloads over the greater Arabian Peninsula
 327 area and a more realistic representation of the spatial distribution of AOD compared to the
 328 corresponding MODIS satellite retrievals. These findings support the previous results by Kim et
 329 al., 2013 who also showed an increase in dust emissions and a more realistic comparison with
 330 satellite observations in Saudi Arabia by the introduction of an NDVI based dynamic source
 331 mapping for GOCART model. Comparison with AERONET measurements also showed significant
 332 improvement especially at higher AODs that are also relevant to the model efficiency for air
 333 quality purposes (i.e. the model bias is reduced from -0.140 to 0.083 at AOD>0.25 and from -
 334 0.933 to -0.424 at AOD>1). However, the model statistics are not improved for all AERONET
 335 measuring stations and for all air quality states (Table2), mainly due to a possible
 336 misclassification of dust sources in the highlands of Iran and Pakistan.

337 The main purpose of our work was the development and first testing of this new modeling
 338 version. A major advance of our study is the ability to implement the real-time properties of
 339 dust sources in air quality simulations (as represented by the satellite NDVI) and thus capture

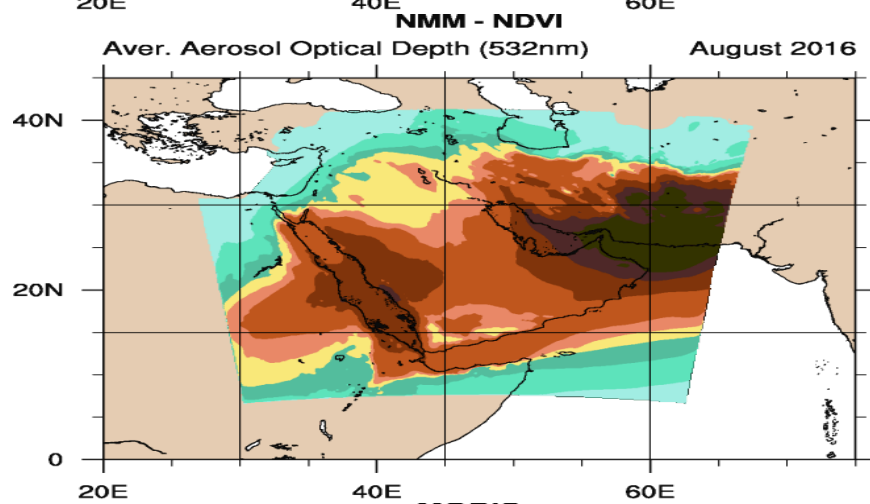
340 local or seasonal effects. In general, one year is not sufficient for extracting robust statistical
 341 results and further analysis is required to examine the performance of the proposed
 342 methodology over longer time periods and also over different areas worldwide. For example
 343 the simple approach of employing a uniform value of NDVI<0.1 for determining the active dust
 344 sources may not be adequate to represent fine-scale land properties and further adjustments
 345 may be required depending on local-scale characteristics. This new approach for the dynamic
 346 characterization of active dust sources based on NDVI can be easily implemented in other
 347 atmospheric dust models at different configurations and spatial coverage for improving their
 348 performance.

349 **Table 2. Statistical metrics from the annual runs (2016) at AERONET stations. Bold values indicate correlation**
 350 **coefficient with p <0.01.**

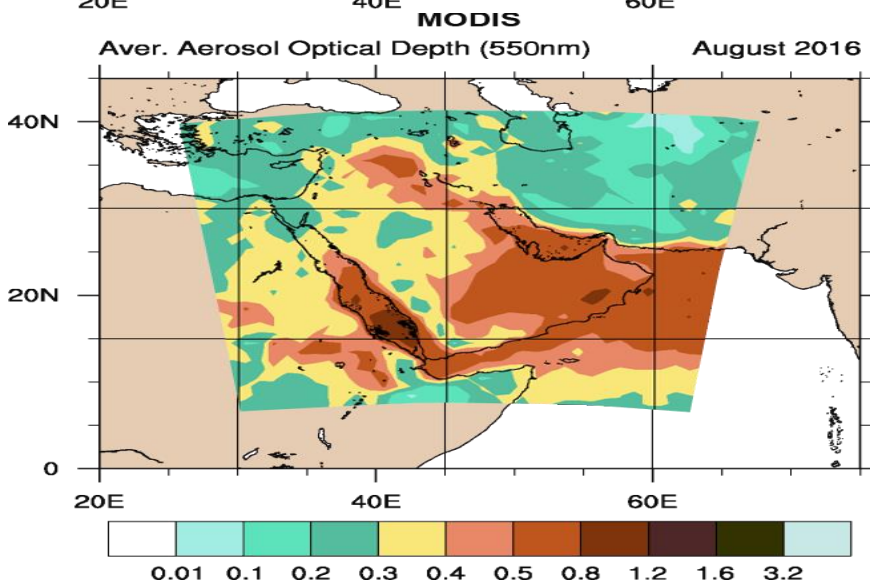
Station	Mean bias		RMSE		Correlation		Fractional gross error		Mean fractional bias	
	CTRL	NDVI	CTRL	NDVI	CTRL	NDVI	CTRL	NDVI	CTRL	NDVI
AgiaMarina_Xyliatou	-0.188	-0.185	0.226	0.224	-0.005	0.001	1.825	1.780	-1.828	-1.767
Cairo_EMA_2	-0.355	-0.344	0.406	0.399	-0.053	0.018	1.689	1.646	-1.687	-1.591
Eilat	-0.138	0.006	0.186	0.165	0.110	0.312	1.183	0.610	-1.166	0.034
El_Farafra	-0.186	-0.190	0.259	0.263	0.170	0.138	1.155	1.248	-1.218	-1.257
KAUST_Campus	-0.245	0.152	0.322	0.376	0.412	0.386	0.966	0.609	-1.001	0.342
Kuwait_University	-0.097	0.007	0.275	0.278	0.152	0.266	0.588	0.537	-0.290	0.018
Mezaira	-0.130	0.161	0.228	0.347	0.353	0.445	0.528	0.475	-0.382	0.332
SEDE_BOKER	-0.151	-0.125	0.198	0.201	0.030	0.034	1.202	1.209	-1.228	-0.921
Weizmann_Institute	-0.207	-0.180	0.264	0.255	-0.088	-0.100	1.494	1.323	-1.521	-1.197



352

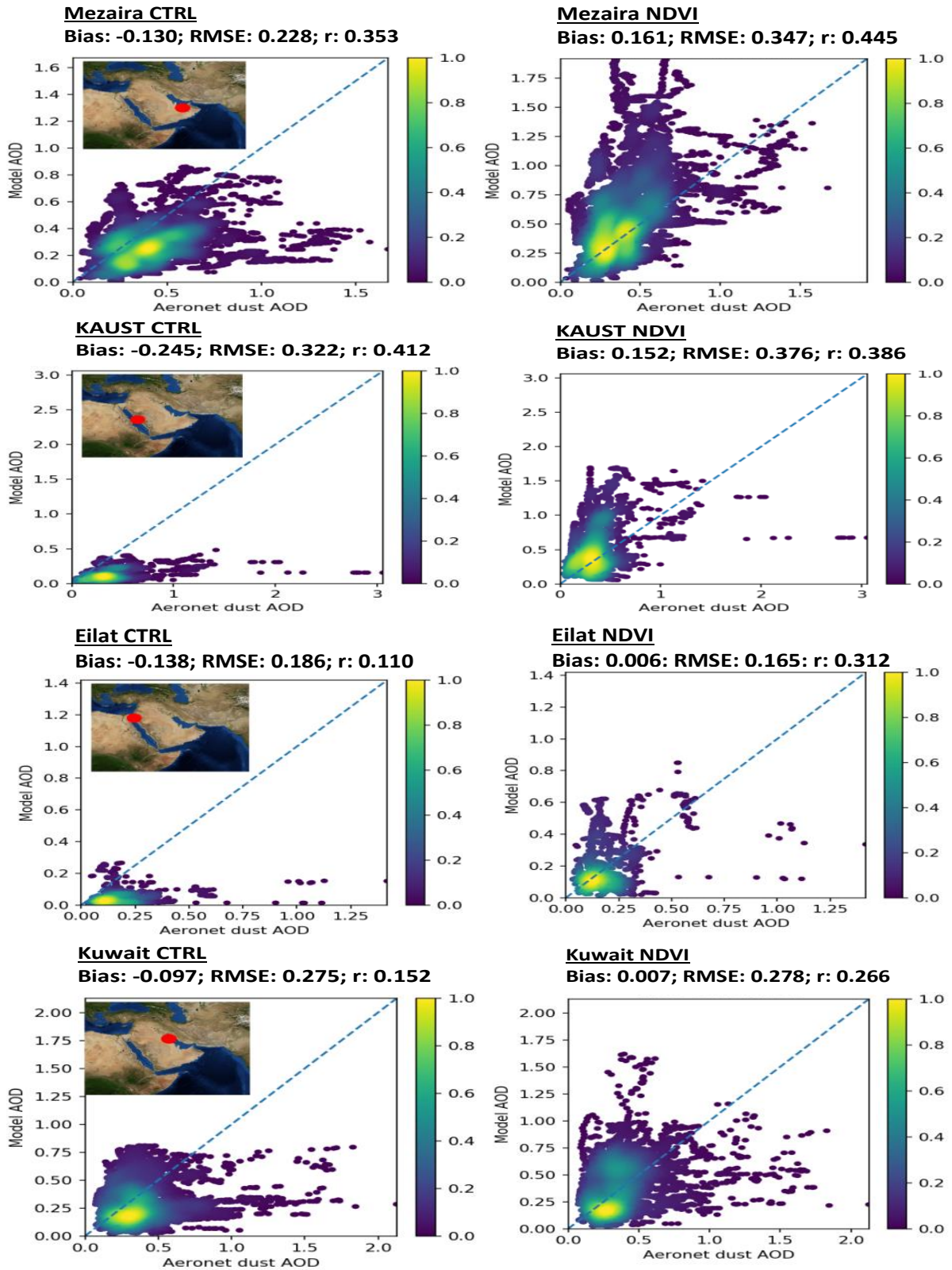


353



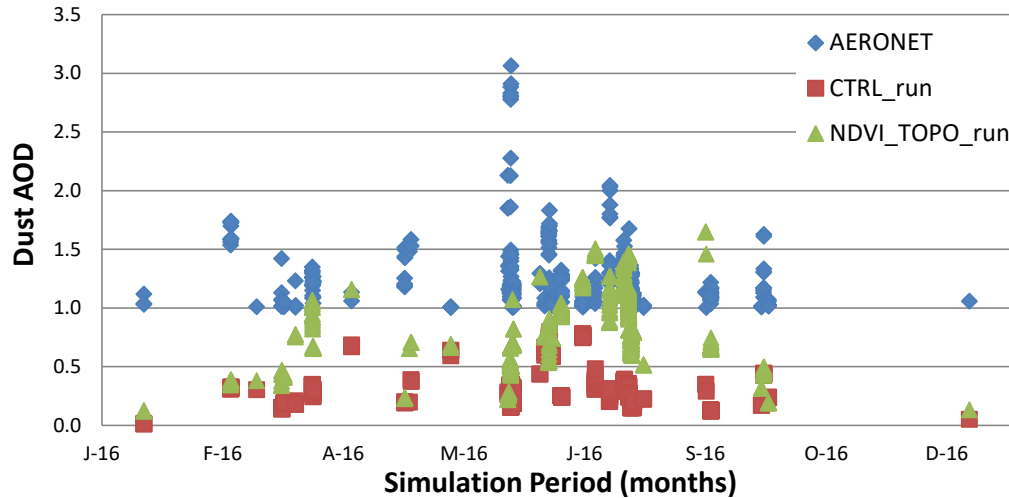
354

355 Figure 4. Monthly average simulated AOD during August 2016 from DREAM-CTRL run (a),
 356 DREAM-NDVI run (b) and (c) MODIS. The dashed trapezoid in (c) denotes the location of the
 357 modeling domain.



358

359 Figure 5. Density scatter plots of modeled and AERONET dust AOD at the stations of Mezaira,
 360 Kuwait, Eilat and Kuwait for 2016.



361
 362 Figure 6. Timeseries of measured and modeled dust AOD for the cases of AERONET AOD>1
 363

364 **Code and Data availability**

365 All code and data used in this study are available upon request.

366 **Author Contribution**

367 SS: Conceptualization, Formal analysis, Investigation, Methodology, Project administration,
 368 Resources, Software, Validation, Visualization, Writing - original draft, Writing – review &
 369 editing;

370 AA: Conceptualization, Funding acquisition, Project administration, Supervision, Writing –
 371 review & editing;

372 CS: Software, Data curation, Visualization, Writing – review & editing;

373 IB: Conceptualization, Formal analysis, Software, Writing – review & editing;

374 SN: Methodology, Supervision, Writing – review & editing;

375 **Acknowledgements**

376 This work was funded by a grant from the National Space Science and Technology Center of the
 377 United Arab Emirates University under grant number NSS Center 7 -2017.The authors
 378 acknowledge also support from BEYOND Centre of Excellence (FP7-REGPOT-2012-2013-1, grant
 379 agreement no. 316210) for providing financial support and computing resources.

380

381 **References**

- 382 Almazrouia, M., M. Nazrullslama, P.D. Jonesa, H. Athara and M. AshfaqrRahmana: Recent
383 climate change in the Arabian Peninsula: Seasonal rainfall and temperature climatology of Saudi
384 Arabia for 1979–2009. *Atmospheric Research*, 111, July 2012, p.p. 29–45., 2012
- 385 Anderson, J., E. Hardy, J. Roach, and R. Witmer: A land use and land cover classification
386 system for use with remote sensing data, U.S. Geol. Prof. Pap. 964, U.S. Gov. Print.Off.,
387 Washington, D. C., 1976
- 388 Anisimov, A., Tao, W., Stenchikov, G., Kalenderski, S., Prakash, P. J., Yang, Z.-L., and Shi, M.:
389 Quantifying local-scale dust emission from the Arabian Red Sea coastal plain, *Atmos. Chem.*
390 *Phys.*, 17, 993-1015, <https://doi.org/10.5194/acp-17-993-2017>, 2017
- 391 Arindam, C., Ravi, S., Nanjundiah and J.: Srinivasan, Impact of African orography and the
392 Indian summer monsoon on the low-level Somali jet, *Int. J. Climatol.* 29: 983–992 (2009), DOI:
393 10.1002/joc.1720, 2009
- 394 Boylan, J. W. and Russell, A. G.: PM and light extinction model performance metrics, goals,
395 and criteria for three-dimensional air quality models, *Atmos. Environ.*, 40(26), 4946–4959,
396 doi:10.1016/j.atmosenv.2005.09.087, 2006.
- 397 Brown, M. E., J. E. Pinzon, K. Didan, J. T. Morisette, and C. J. Tucker (2006), Evaluation of the
398 consistency of long-term NDVI time series derived from AVHRR, SPOT-Vegetation, SeaWiFS,
399 MODIS and Land-SAT ETM+, *IEEE Trans. Geosci. Remote Sens.*, 44, 1787–1793.
- 400 Chang, J. C. and Hanna, S. R.: Air quality model performance evaluation, *Meteorol Atmos*
401 *Phys*, 87(1–3), 167–196, doi:10.1007/s00703-003-0070-7, 2004.
- 402 DeFries, R. S., and Townshend, J. R. G.: NDVI-derived land cover classifications at a global
403 scale, *Int. J. Remote Sens.*, 15, 3567–3586, doi:10.1080/01431169408954345, 1994.
- 404 Didan, K. : MOD13A1 MODIS/Terra Vegetation Indices 16-Day L3 Global 500m SIN Grid V006
405 [Data set].NASA EOSDIS LP DAAC.doi: 10.5067/MODIS/MOD13A1.006, 2015
- 406 Didan, K.; Munoz, A.B.; Solano, R.; Huete, A. MODIS Vegetation Index User’s Guide (MOD13
407 Series); Version3.0; University of Arizona: Tucson, AZ, USA, 2015.
- 408 Esmail N., M. Gharagozloo, A. Rezaei, G. Grunig: Dust events, pulmonary diseases and
409 immune system, *Am J ClinExplImmunol* 2014 3(1):20-29, 2014.
- 410 Georgi, F. A particle dry-deposition parameterization scheme for in tracer transport models,
411 *Journal of Geophysical Research*, 91, 9794 – 9806, 1986
- 412 Ginoux, P., Chin, M., Tegen, I., Prospero, J. M., Holben, B., Dubovik, O., & Lin, S.-J.: Sources
413 and distributions of dust aerosols simulated with the GOCART model. *Journal of Geophysical*
414 *Research*, 106(D17), 20,255–20,273. <https://doi.org/10.1029/2000JD000053>, 2001
- 415 Ginoux, P., J. M. Prospero, T. E. Gill, N. C. Hsu, and M. Zhao (2012), Global-scale attribution of
416 anthropogenic and natural dust sources and their emission rates based on MODIS Deep Blue
417 aerosol products, *Rev. Geophys.*, 50, RG3005 doi:10.1029/2012RG000388.
- 418 Holben, B.N., Eck, T.F., Slutsker, I., Tanre, D., Buis, J.P., Setzer, A., Vermote, E., Reagan, J.A.,
419 Kaufman, Y., Nakajima, T., Lavenu, F., Jankowiak, I., Smirnov, A.: AERONET a federated
420 instrument network and data archive for aerosol characterization. *Rem. Sens. Environ.* 66,
421 1e16., 1998

422 Huete, A. R., Justice, C., and van Leeuwen, W., MODIS Vegetation index (MOD 13): Algorithm
423 Theoretical Basis Document, NASA Goddard Space Flight Center, Greenbelt, Maryland 20771,
424 1999

425 Huete, A., Didan, K., Miura, T., Rodriguez, E. P., Gao, X., & Ferreira, L. G.: Overview of the
426 radiometric and biophysical performance of the MODIS vegetation indices. *Remote Sensing of*
427 *Environment*, 83, 195–213., 2002

428 Janjic, Z.I., Gerrity J.P.Jr., and *Nickovic, S.*: An Alternative Approach to Nonhydrostatic
429 Modeling. *Monthly Weather Review*, 129: 1164-1178., 2001

430 Kim, D., M. Chin, H. Bian, Q. Tan, M. E. Brown, T. Zheng, R. You, T. Diehl, P. Ginoux, and T.
431 Kucsera: The effect of the dynamic surface bareness on dust source function, emission, and
432 distribution, *J. Geophys. Res. Atmos.*, 118, 871–886, doi: 10.1029/2012JD017907., 2013

433 Kumar, P., Sokolik, I. N., and Nenes, A.: Measurements of cloud condensation nuclei activity
434 and droplet activation kinetics of fresh unprocessed regional dust samples and minerals,
435 *Atmos. Chem. Phys.*, 11, 3527–3541, doi:10.5194/acp-11-3527-2011, 2011.

436 Mahowald, N, Albani, S., Kok, J. F., Engelstaeder, S., Scanza, R., Ward, D.S., Flanner, M.G.:The
437 size distribution of desert dust aerosols and its impact on the Earth system, *Aeolian Research*,
438 15, 2014, Pages 53-71, <https://doi.org/10.1016/j.aeolia.2013.09.002.>, 2014

455 Mamouri, R.-E., Ansmann, A., Nisantzi, A., Solomos, S., Kallos, G., and Hadjimitsis, D. G.:
456 Extreme dust storm over the eastern Mediterranean in September 2015: satellite, lidar, and
457 surface observations in the Cyprus region, *Atmos. Chem. Phys.*, 16, 13711-13724,
458 <https://doi.org/10.5194/acp-16-13711-2016>, 2016

459 Mitsakou, C., Kallos, G., Papantoniou, N., Spyrou, C., Solomos, S., Astitha, M., and Housiadas,
460 C.: Saharan dust levels in Greece and received inhalation doses, *Atmos. Chem. Phys.*, 8, 7181-
461 7192, <https://doi.org/10.5194/acp-8-7181-2008>, 2008.

462 Nickovic, S., G. Kallos, A. Papadopoulos, and O. Kakaliagou: A model for prediction of desert
463 dust cycle in the atmosphere, *J. Geophys. Res.*, 106(D16), 18,113–18,129, 2001

464 Nickovic, S., Cvetkovic, B., Madonna, F., Rosoldi, M., Pejanovic, G., Petkovic, S., and Nikolic,
465 J.: Cloud ice caused by atmospheric mineral dust – Part 1: Parameterization of ice nuclei
466 concentration in the NMME-DREAM model, *Atmos. Chem. Phys.*, 16, 11367-11378,
467 <https://doi.org/10.5194/acp-16-11367-2016>, 2016.

468 Olson, J. S., J. A. Watts and L. J. Allison: Carbon in Live Vegetation of Major World
469 Ecosystems, Report ORNL-5862, Oak Ridge National Laboratory, Oak Ridge, Tennessee, USA.,
470 1983

471 Parajuli S.P., Zender C.S., Connecting geomorphology to dust emission through high-
472 resolution mapping of global land cover and sediment supply, *Aeolian Research* 27, 47-65,
473 doi:10.1016/j.aeolia.2017.06.002

474 Pejanovic, G., S. Nickovic, M. Vujadinovic, A. Vukovic, V. Djurdjevic, M. Dacic: Atmospheric
475 deposition of minerals in dust over the open ocean and possible consequences on climate.
476 WCRP OSC Climate Research in Service to Society, 24-28 October 2011, Denver, CO, USA, 2011

477 Pérez, C., S. Nickovic, J. M. Baldasano, M. Sicard, F. Rocaadenbosch, and V. E. Cachorro: A long
478 Saharan dust event over the western Mediterranean: Lidar, Sun photometer observations, and
479 regional dust modeling, *J. Geophys. Res.*, 111, D15214, doi:10.1029/2005JD006579., 2006

480 Platnick, S., et al., 2017. MODIS Atmosphere L3 Monthly Product. NASA MODIS Adaptive
481 Processing System, Goddard Space Flight Center, USA:
482 http://dx.doi.org/10.5067/MODIS/MOD08_M3.061

483 Prospero J. M., P. Ginoux, O. Torres, S. E. Nicholson, and T. E. Gill: Environmental
484 characterization of global sources of atmospheric soil dust identified with the nimbus 7 total
485 ozone mapping spectrometer (TOMS) absorbing aerosol product, *Rev. Geophys.*, 40(1), 1002,
486 doi:10.1029/2000RG000095, 2002

487 Rouse Jr, R. H. Haas, J. A. Schell, and D. W. Deering: "Monitoring vegetation systems in the
488 Great Plains with ERTS." In NASA. Goddard Space Flight Center 3d ERTS-1 Symp., Vol. 1, Sect. A p
489 309-317, 1974

490 Solano, R., K. Didan, A., Jacobson and A. Huete: MODIS Vegetation Index User's Guide, ver.
491 2.0, Vegetation Index and Phenology Lab, <http://vip.arizona.edu>, The University of Arizona.,
492 2010

493 Solomos, S., Kallos, G., Kushta, J., Astitha, M., Tremback, C., Nenes, A., and Levin, Z.: An
494 integrated modeling study on the effects of mineral dust and sea salt particles on clouds and
495 precipitation, *Atmos. Chem. Phys.*, 11, 873–892, doi:10.5194/acp-11-873-2011, 2011.

496 Solomos, S., Ansmann, A., Mamouri, R.-E., Biniotoglou, I., Patlakas, P., Marinou, E., and
497 Amiridis, V.: Remote sensing and modelling analysis of the extreme dust storm hitting the
498 Middle East and eastern Mediterranean in September 2015, *Atmos. Chem. Phys.*, 17, 4063-
499 4079, <https://doi.org/10.5194/acp-17-4063-2017>, 2017

500 Spyrou, C.: Direct radiative impacts of desert dust on atmospheric water content, *Aerosol*
501 *Science and Technology*, DOI: 10.1080/02786826.2018.1449940., 2018

502 Spyrou, C., G. Kallos, C. Mitsakou, P. Athanasiadis, C. Kalogeri and M. J. Iacono, 2013:
503 Modeling the radiative effects of desert dust on weather and regional climate. *Atmos. Chem.*
504 *Phys.*, 13, 5489–5504, doi:10.5194/acp-13-5489-2013, 2013

505 Spyrou, C., C. Mitsakou, G. Kallos, P. Louka, and G. Vlastou: An improved limited area model
506 for describing the dust cycle in the atmosphere, *J. Geophys. Res.*, 115, D17211,
507 doi:10.1029/2009JD013682., 2010

508 Torge, A., Macke, A., Heinold, B. and Wauer, J.: Solar radiative transfer simulations in
509 Saharan dust plumes: particle shapes and 3-D effect. *Tellus B*, 63: 770-780. doi:10.1111/j.1600-
510 0889.2011.00560.x, 2011

511 Tucker, C. J., J. E. Pinzon, M. E. Brown, D. Slayback, E.W. Pak, R. Mahoney, E. Vermote, and N.
512 El Saleous (2005), An extended AVHRR 8-km NDVI data set compatible with MODIS and SPOT
513 vegetation NDVI data, *Int. J. Remote Sens.*, 26, 4485–4498.

514 Vukovic, A., Vujadinovic, M., Pejanovic, G., Andric, J., Kumjian, M. R., Djurdjevic, V., Dacic,
515 M., Prasad, A. K., El-Askary, H. M., Paris, B. C., Petkovic, S., Nickovic, S., and Sprigg, W. A.:
516 Numerical simulation of "an American haboob", *Atmos. Chem. Phys.*, 14, 3211-3230,
517 <https://doi.org/10.5194/acp-14-3211-2014>, 2014

518 Walko RL, Band LE, Baron J, Kittel TGF, Lammers R, Lee TJ, Ojima D, Pielke RA Sr, Taylor C,
519 Tague C, Tremback CJ, Vidale PJ, Coupled atmosphere-biophysichydrology models for
520 environmental modeling. *J Appl Meteor* 39: 931–944, 2000

521 Xue Y., Sellers P. J., Kinter J. L., and Shukla J.: A simplified biosphere model for global climate
522 studies *J. Clim.* 4 345–64, 1991